conclude that the soluble UGT85B1 interacts with both CYP79A1 and CYP71E1, but that it is not necessary for CYP79A1-CYP71E1 complex formation (Fig. 4E). CYP79A1, CYP71E1, CYP98A1, and POR2b are situated very close together at the ER surface and have comparable pairwise FRET values (Fig. 4F and table S11). All microsomal P450s require electron donation from POR; therefore, it is not surprising that CYP98A1 is proximal to the dhurrin biosynthetic enzymes (Fig. 4, A, B, and D). UGT85B1 was situated close to the nonpartner ER membrane proteins, CYP98A1 and POR2b, when CYP79A1 and CYP71E1 were coexpressed (table S12).

A prerequisite to understanding how cells coordinate diverse metabolic activities is to understand how the enzyme systems catalyzing these reactions are organized and their possible enrollment as part of dynamic metabolons. Efforts to maximize product yield from genetically engineered pathways (14–17) would benefit from this information. In this study, we showed that the dhurrin pathway forms an efficient metabolon. CYP79A1 and CYP71E1 form homo- and hetero-oligomers, which enable recruitment of the cytosolic soluble UGT85B1 (Fig. 4G). UGT85B1 regulates the flux of L-tyrosine and stimulates channeling between CYP79A1 and CYP71E1. Efficient metabolic flux and channeling require an overall negatively charged lipid surface and may provide an additional means for regulating the dynamic assembly necessary to respond swiftly to environmental challenges. A similar organization may characterize the biosynthetic pathways of other specialized metabolites as well.

REFERENCES AND NOTES

1. R. M. Gleadow, B. L. Møller, *Annu. Rev. Plant Biol.* **65**, 155–185 (2014).
2. T. Laursen, B. L. Møller, J. E. Bassard, *Trends Plant Sci.* **20**, 20–32 (2015).
3. B. A. Halkier, B. L. Møller, *Plant Physiol.* **90**, 1552–1559 (1989).
4. O. Sibbesen, B. Koch, B. A. Halkier, B. L. Møller, *Proc. Natl. Acad. Sci. U.S.A.* **91**, 9740–9744 (1994).
5. B. L. Møller, *Science* **330**, 1328–1329 (2010).
6. K. Jørgensen et al., *Curr. Opin. Plant Biol.* **8**, 280–291 (2005).
7. S. An, R. Kumar, E. D. Sheets, S. J. Benkovic, *Science* **320**, 103–106 (2008).
8. K. Mohr, E. Kostenis, *Nat. Chem. Biol.* **7**, 860–861 (2011).
9. S. C. Lee et al., *Nat. Protoc.* **11**, 1149–1162 (2016).
10. T. Laursen et al., *ACS Chem. Biol.* **9**, 630–634 (2014).
11. Materials and methods are available as supplementary materials on *Science* Online.
12. H. M. Ting et al., *New Phytol.* **199**, 352–366 (2013).
13. J. E. Bassard et al., *Plant Cell* **24**, 4465–4482 (2012).
14. I. Wheeldon et al., *Nat. Chem.* **8**, 299–309 (2016).
15. C. Singleton, T. P. Howard, N. Smirnoff, *J. Exp. Bot.* **65**, 1947–1954 (2014).
16. G. Farré et al., *Annu. Rev. Plant Biol.* **65**, 187–223 (2014).
17. J. E. Dueber et al., *Nat. Biotechnol.* **27**, 753–759 (2009).

NEURODEVELOPMENT

The sacral autonomic outflow is sympathetic

I. Espinosa-Medina,[1]* O. Saha,[1]* F. Boismoreau,[1] Z. Chettouh,[1] F. Rossi,[1] W. D. Richardson,[2] J.-F. Brunet[1]†

A kinship between cranial and pelvic visceral nerves of vertebrates has been accepted for a century. Accordingly, sacral preganglionic neurons are considered parasympathetic, as are their targets in the pelvic ganglia that prominently control rectal, bladder, and genital functions. Here, we uncover 15 phenotypic and ontogenetic features that distinguish pre- and postganglionic neurons of the cranial parasympathetic outflow from those of the thoracolumbar sympathetic outflow in mice. By every single one, the sacral outflow is indistinguishable from the thoracolumbar outflow. Thus, the parasympathetic nervous system receives input from cranial nerves exclusively and the sympathetic nervous system from spinal nerves, thoracic to sacral inclusively. This simplified, bipartite architecture offers a new framework to understand pelvic neurophysiology as well as development and evolution of the autonomic nervous system.

The allocation of the sacral autonomic outflow to the parasympathetic division of the visceral nervous system—as the second tier of a "cranio-sacral outflow"—has an ancient origin, yet a simple history: It is rooted in the work of Gaskell (1), was formalized by Langley (2), and has been universally accepted ever since [as in (3)]. The argument derived from several similarities of the sacral outflow with the cranial outflow: (i) anatomical—a target territory less diffuse than that of the thoracolumbar outflow, a separation from it by a gap at limb levels, and a lack of projections to the paravertebral sympathetic chain (1); (ii) physiological—an influence on some organs opposite to that of the thoracolumbar outflow (4); and (iii) pharmacological—an overall sensitivity to muscarinic antagonists (2). However, analysis of cellular phenotype was lacking. Here, we define differential genetic signatures and dependencies for parasympathetic and sympathetic neurons, both pre- and postganglionic. When we reexamine the sacral autonomic outflow of mice in this light, we find that it is better characterized as sympathetic than parasympathetic.

Cranial parasympathetic preganglionic neurons are born in the "pMNv" progenitor domain of the hindbrain (5) that expresses the homeogene *Phox2b* and produces, in addition, branchiomotor neurons (6). The postmitotic precursors migrate dorsally (7) to form nuclei (such as the dorsal motor nucleus of the vagus nerve) and project through dorsolateral exit points (7) in several branches of the cranial nerves to innervate parasympathetic and enteric ganglia. In contrast, thoracic and upper lumbar (hereafter "thoracic") preganglionic neurons, which are sympathetic, are thought to have a common origin with somatic motoneurons (8, 9). By implication, they would be born in the pMN progenitor domain (just dorsal to p3)—thus from progenitors that express the basic helix-loop-helix (bHLH) transcription factor Olig2 (10). The sympathetic preganglionic precursors then segregate from somatic motoneurons to form the intermediolateral column in mammals (11), project in the ventral roots of spinal nerves together with axons of somatic motoneurons, and, via the white rami communicantes, synapse onto neurons of the paravertebral and prevertebral sympathetic ganglia.

We sought to compare the genetic makeup and dependencies of lower lumbar and sacral (hereafter "sacral") preganglionic neurons with that of cranial (parasympathetic) and thoracic (sympathetic) ones. As representative of cranial preganglionic neurons, we focused on the dorsal motor nucleus of the vagus nerve, a cluster of

[1]Institut de Biologie de l'École Normale Supérieure (IBENS), INSERM, CNRS, École Normale Supérieure, Paris Sciences et Lettres Research University, Paris, 75005 France. [2]Wolfson Institute for Biomedical Research, University College London, London, UK.
*These authors contributed equally to this work †Corresponding author. Email: jfbrunet@biologie.ens.fr
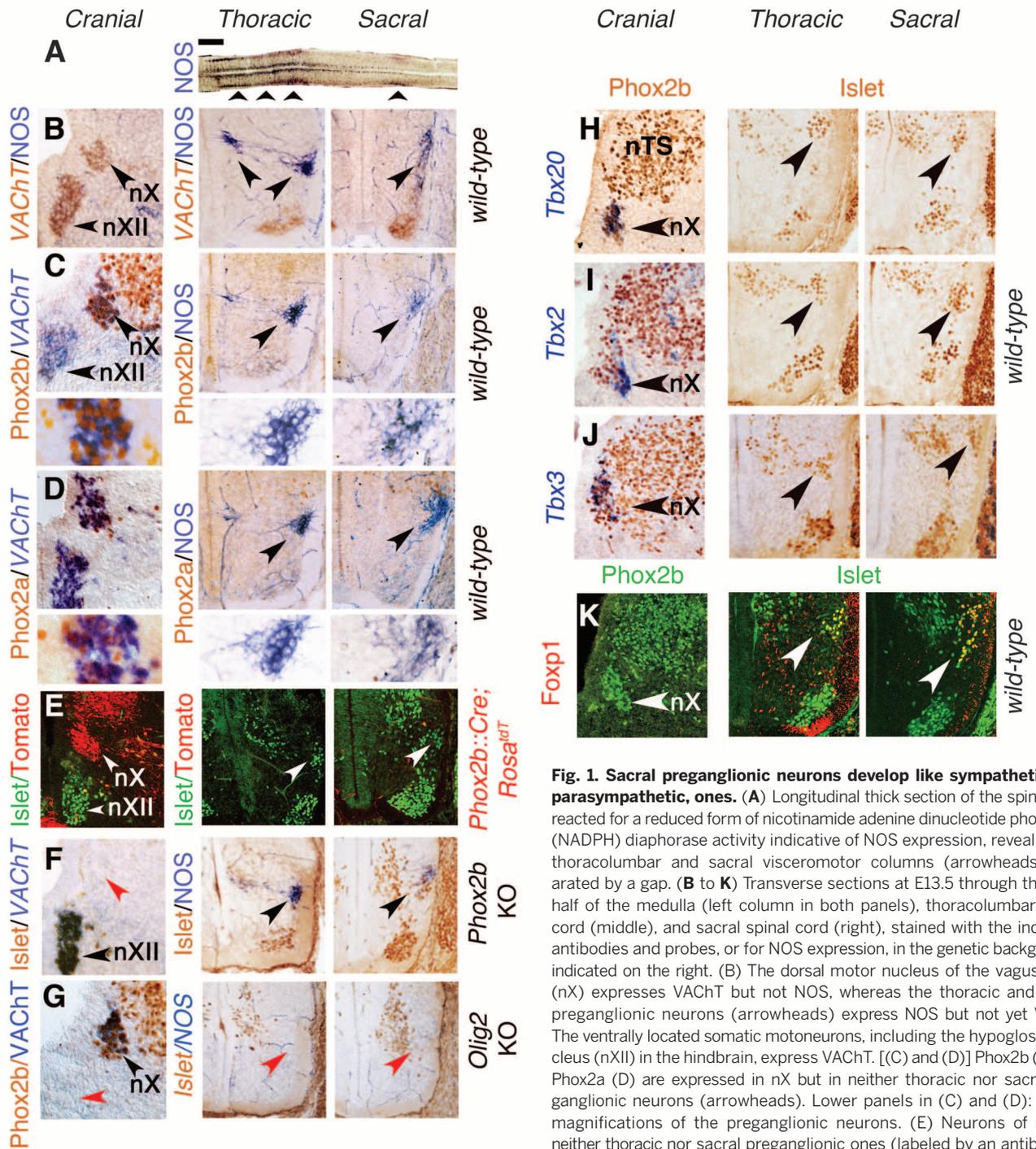
Fig. 1. Sacral preganglionic neurons develop like sympathetic, not parasympathetic, ones. (**A**) Longitudinal thick section of the spinal cord reacted for a reduced form of nicotinamide adenine dinucleotide phosphate (NADPH) diaphorase activity indicative of NOS expression, revealing the thoracolumbar and sacral visceromotor columns (arrowheads) separated by a gap. (**B** to **K**) Transverse sections at E13.5 through the right half of the medulla (left column in both panels), thoracolumbar spinal cord (middle), and sacral spinal cord (right), stained with the indicated antibodies and probes, or for NOS expression, in the genetic backgrounds indicated on the right. (B) The dorsal motor nucleus of the vagus nerve (nX) expresses VAChT but not NOS, whereas the thoracic and sacral preganglionic neurons (arrowheads) express NOS but not yet VAChT. The ventrally located somatic motoneurons, including the hypoglossal nucleus (nXII) in the hindbrain, express VAChT. [(C) and (D)] Phox2b (C) and Phox2a (D) are expressed in nX but in neither thoracic nor sacral preganglionic neurons (arrowheads). Lower panels in (C) and (D): higher magnifications of the preganglionic neurons. (E) Neurons of nX but neither thoracic nor sacral preganglionic ones (labeled by an antibody to Islet1/2, white arrowheads) derive from Phox2b^{+} precursors, permanently labeled in a Phox2b::Cre;Rosa[tdT] background. (F) nX is missing in Phox2b knockouts (red arrowhead), but thoracic and sacral preganglionic neurons are spared (black arrowheads). (G) nX is spared in Olig2 knockouts (black arrowhead), but thoracic and sacral preganglionic neurons are missing (red arrowheads). nXII is also missing, as expected of a somatic motor nucleus (red arrowhead). [(H) to (J)] Tbx20, Tbx2, and Tbx3 are expressed in all or a subset of nX neurons (arrowheads in panels of the left column) but in no thoracic or sacral preganglionic neuron (arrowheads in panels of the middle and right columns). (K) Foxp1 is not expressed in the nX (arrowhead in left column) but is a marker of both thoracic and sacral preganglionic neurons (arrowheads in middle and right columns). nTS, nucleus of the solitary tract. Scale bars: 1 mm (A), 100 μm [(B) to (K)].

neurons already well delineated at 13.5 days of embryonic development (E13.5), that expresses the vesicular acetylcholine transporter (VAChT) (Fig. 1B). Thoracic and sacral preganglionic neurons, which both form a mediolateral column in

the spinal cord, did not express VAChT at this stage despite their eventual cholinergic nature. To localize them, we thus used their common marker nitric oxide synthase (NOS) (*12*) (Fig. 1, A and B), which was absent from the dorsal motor nucleus

of the vagus nerve at E13.5 (Fig. 1B) or later (fig. S1). Thus, NOS expression characterizes thoracic and sacral, but not cranial, preganglionic neurons.

In contrast to cranial (parasympathetic) preganglionic neurons, thoracic (sympathetic) ones
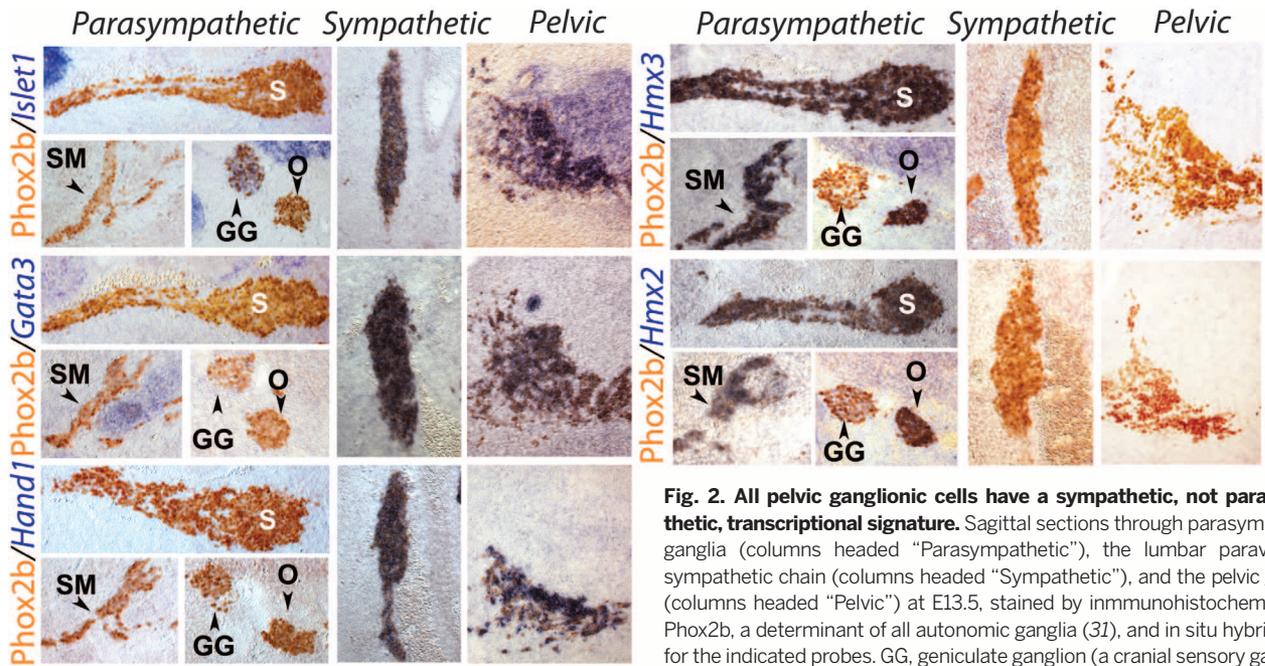
Fig. 2. All pelvic ganglionic cells have a sympathetic, not parasympathetic, transcriptional signature. Sagittal sections through parasympathetic ganglia (columns headed "Parasympathetic"), the lumbar paravertebral sympathetic chain (columns headed "Sympathetic"), and the pelvic ganglion (columns headed "Pelvic") at E13.5, stained by inmmunohistochemistry for Phox2b, a determinant of all autonomic ganglia (*31*), and in situ hybridization for the indicated probes. GG, geniculate ganglion (a cranial sensory ganglion); O, otic ganglion; S, sphenopalatine ganglion; SM, submandibular ganglion (all parasympathetic ganglia).

Fig. 3. The pelvic ganglion forms independently of its nerve, like sympathetic and unlike parasympathetic ones. (**A** and **C**). Whole-mount immunofluorescence with the indicated antibodies on E11.5 embryos either heterozygous (A) or homozygous (C) for an *Olig2* null mutation. The nascent pelvic nerves [yellow arrowhead in (A)] seem to derive mostly from the L6 nerve at that stage. The Olig2 null mutation (C) spares two thin sensory pelvic projections. The pelvic ganglion (PG) lies ahead of most fibers in both heterozygous and mutant background. (**B** and **D**). View of the L6 nerve, covered with Sox10$^+$ cells but no Phox2b$^+$ cells (yellow arrowheads), unlike cranial nerves that give rise to parasympathetic ganglia at the same stage [Jacobson's nerve in (**E**)]. (**F** and **G**) In situ hybridization for Phox2b and immunohistochemistry for neurofilament (NF) on heterozygous and homozygous Olig2 knockouts at E13.5, when parasympathetic ganglia have formed elsewhere in the body. Graph: the pelvic ganglion has the same volume whether its preganglionic nerve is present [black arrowhead in (F)] or not (6369 μm^3 ± 1066 versus 6441 μm^3 ± 919, *P* = 0.96, *n* = 5 embryos). gt, genital tubercle; L5 and L6, 5th and 6th lumbar roots; S1, 1st sacral root; SC, sympathetic chain.
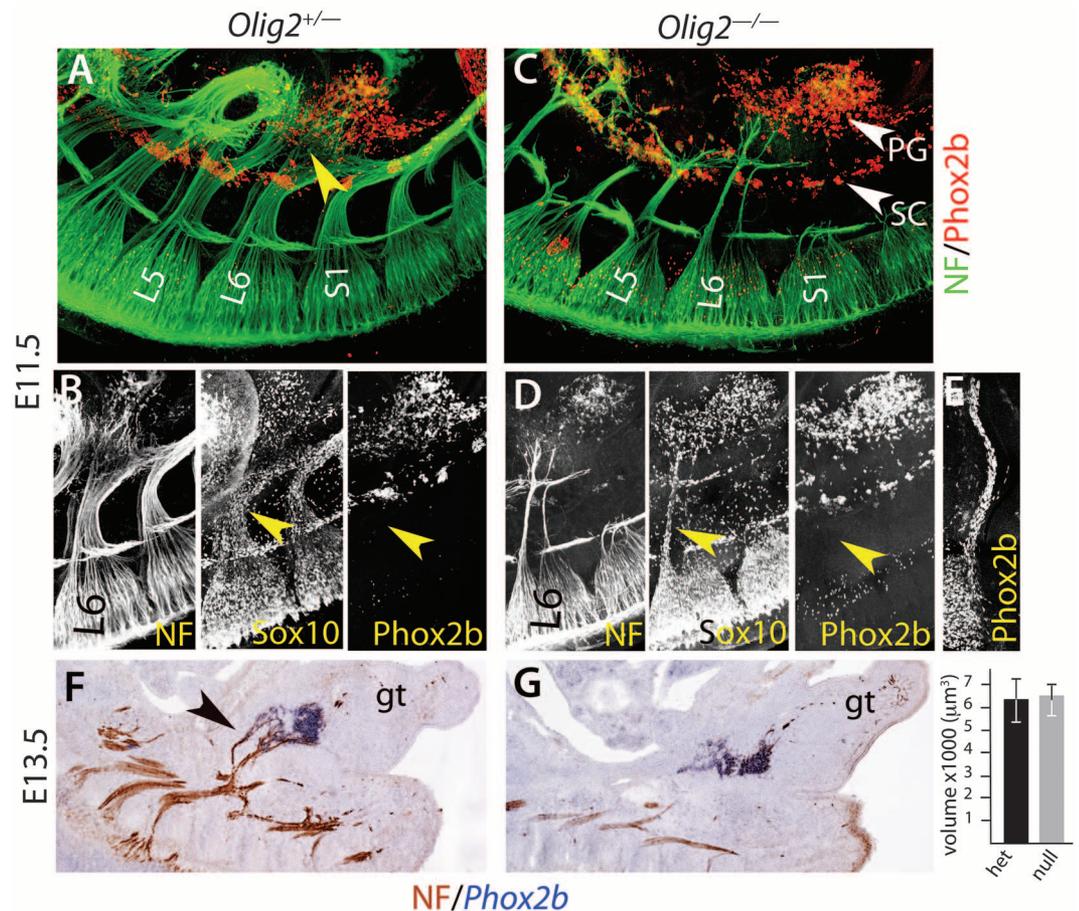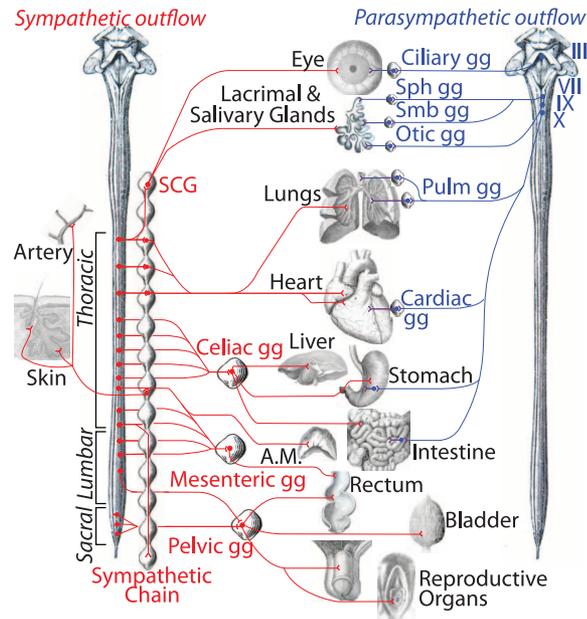
Fig. 4. Revised anatomy of the autonomic nervous system. The efferent path of the autonomic nervous system is made up of a spinal sympathetic outflow (left, in red) and a cranial parasympathetic outflow (right, in blue). Sympathetic targets in the skin other than arteries are piloerector muscles and sweat glands. III, oculomotor nerve; VII, facial nerve; IX, glosso-pharyngeal nerve; X, vagus nerve; A.M., adrenal medulla; gg, ganglion; Pulm, pulmonary; SCG, superior cervical ganglion; Sph, spheno-palatine; Smb, submandibular. For a larger version, see fig. S11.

Sympathetic outflow   *Parasympathetic outflow*

Eye — Ciliary gg, Sph gg

Lacrimal & Salivary Glands — Smb gg, Otic gg

SCG

Lungs — Pulm gg

Artery

Heart — Cardiac gg

Skin

Celiac gg — Liver, Stomach

A.M. — Intestine

Mesenteric gg — Rectum

Pelvic gg — Bladder, Reproductive Organs

Sympathetic Chain

III, VII, IX, X

not only failed to express Phox2b or its paralogue Phox2a at E13.5 but also arose from Phox2b-negative progenitors and did not depend on Phox2b for their differentiation (Fig. 1, C to F, left and middle columns) but instead depended on Olig2 (Fig. 1G). Sacral preganglionic neurons shared all these features with thoracic ones (Fig. 1, C to G, middle and right columns). At E13.5, the T-box transcription factors Tbx20, Tbx2, and Tbx3 were expressed by cranial (parasympathetic) neurons but by neither thoracic (sympathetic) nor sacral preganglionic ones (Fig. 1, H to J, and fig. S2). The F-box transcription factor Foxp1, a determinant of thoracic preganglionic neurons (13), was expressed by sacral but not cranial preganglionic neurons (Fig. 1K). Differential expression of Phox2b, Tbx20, and FoxP1 between cranial and all spinal preganglionic neurons, thoracic and sacral, was still observed at E16.5 (fig. S3). In sum, the ontogeny and transcriptional signature of sacral preganglionic neurons was indistinguishable from that of thoracic ones and therefore sympathetic as well.

Thoracic and sacral preganglionic neurons share a settling site in the mediolateral region of the spinal cord and a ventral exit point for their axons, whereas cranial preganglionics have a less systematized topography and a dorsal axonal exit point. These similarities of thoracic with sacral, and differences of both with cranial, are at odds with the notion of craniosacral outflow since its first description (1).

The targets of the sacral preganglionic neurons are in the pelvic plexus (figs. S4 and S5) and are considered, by definition, parasympathetic (14). Because a proportion of pelvic ganglionic neurons receive input from upper lumbar levels [half of them in rats (15)] and thus from sympathetic preganglionic neurons, the pelvic ganglion is considered mixed sympathetic and parasympathetic (16). This connectivity-based definition runs into a conundrum for cells that receive a dual lumbar/sacral input (17). The sympathetic identity of both thoracic and sacral preganglionic neurons that we unveil here makes the issue moot. Regardless, we looked for a cell-intrinsic criterion that would corroborate the sympathetic nature of all pelvic ganglionic cells in the form of genes differentially expressed in sympathetic versus parasympathetic ganglionic cells elsewhere in the autonomic nervous system. Neurotransmitter phenotypes do not map on the sympathetic/parasympathetic partition because cholinergic neurons in the pelvic ganglion comprise both "parasympathetic" and "sympathetic" ganglionic cells, as defined by connectivity (14), and bona fide sympathetic neurons of the paravertebral chain are cholinergic [reviewed in (18)]. However, we found that three transcription factors expressed and required in the sympathoadrenal lineage—Islet1 (19), Gata3 (20), and Hand1 (21)—were not expressed in para-sympathetic ganglia such as the sphenopalatine, the submandibular, or the otic ganglia (Fig. 2 and fig. S6) [although Islet1 is expressed in ciliary ganglia (22) and Gata3 in cardiac ones (20), which thus diverge from the canonical parasympathetic molecular signature]. Conversely, we found that the two paralogous homeobox genes *Hmx2* and *Hmx3* are specific markers of all parasympathetic versus sympathetic ganglia and adrenal medulla (Fig. 2 and figs. S6 and S7). All cells of the pelvic ganglion were Islet1$^+$, Gata3$^+$, Hand1$^+$, Hmx3$^-$, and Hmx2$^-$ at E13.5 (Fig. 2) and at E16.5 (fig. S8), as were smaller scattered ganglia of the pelvic organs (fig. S8). Thus, all had a sympathetic transcriptional fingerprint. Similarly, the chicken ganglion of Remak, classically considered para-sympathetic (23), displayed an Islet1$^+$, Hand1$^+$, Hmx3$^-$ signature, and thus is sympathetic (fig. S9).

Finally, we tested the pelvic ganglion for the contrasted modes of development of sympathetic and parasympathetic ganglia. Parasympathetic ganglia, unlike sympathetic ones, arise through the migration of Sox10$^+$/Phox2b$^+$ Schwann cell precursors along their future preganglionic nerve toward the site of ganglion formation and do not form if these nerves are absent (24, 25). At E11.5, the lumbosacral plexus, which gives rise to the pelvic nerve, extended some fibers that reached the lateral and rostral edge of the pelvic ganglion anlagen, most of which was already situated well ahead of them (Fig. 3A and movie S1). These fibers were coated with Sox10$^+$ cells, none of which, though, expressed Phox2b (Fig. 3B), in contrast to the cranial nerves that produce parasympathetic ganglia at the same stage (Fig. 3E). Deletion of all motor fibers in Olig2$^{-/-}$ embryos spared only two thin, presumably sensory, projections from the lumbosacral plexus (Fig. 3C), also devoid of Phox2b$^+$ cells (Fig. 3D and fig. S10). Despite this massive atrophy, the pelvic ganglion appeared intact (Fig. 3C, fig. S10, and movie S2). This was verified quantitatively at E13.5 (Fig. 3, F and G). Thus, even though 50% of its cells are post-ganglionic to the pelvic nerve, the pelvic ganglion forms before and independently of it, as befits a sympathetic ganglion but contrary to parasym-pathetic ones.

Thus, the sacral visceral nervous system is the caudal outpost of the sympathetic outflow (Fig. 4 and fig. S11), the autonomic nervous system being divided in a cranial and a spinal autonomic system, in line with certain evolutionary speculations (26). This new understanding of the anatomy accounts for many data that were at odds with the previous one. For example, although schematics generally represent the sacral pathway to the rectum as disynaptic—i.e., vagal-like—[e.g., (3)], it is in fact predominantly (27) if not exclusively (28) trisynaptic—i.e., sympathetic-like (29). Despite the dogma of lumbosacral antagonism on the bladder detrusor muscle, the lumbar inhibition is experimentally absent (4) or of dubious functional relevance (30). The synergy of the lumbar and sacral pathway for vasodilatation in external sexual organs [reviewed in (29)] shows a continuity of action—rather than antagonism, as the old model suggested—across the gap between the thoracolumbar and sacral outflows.

The sympathetic identity of all sacral and pelvic autonomic neurons, which our data unveil, pro-vides a new framework for discoveries on pelvic neuroanatomy and physiology.

REFERENCES AND NOTES

1. W. H. Gaskell, *J. Physiol.* **7**, 1–80.9 (1886).
2. J. N. Langley, *The Autonomic Nervous System: Part I* (W. Heffer, Cambridge, 1921).
3. E. Kandel, J. Schwartz, T. Jessell, S. Siegelbaum, A. J. Hudspeth, *Principles of Neural Science, Fifth Edition* (McGraw-Hill Professional, 2012).
4. J. N. Langley, H. K. Anderson, *J. Physiol.* **19**, 71–139 (1895).
5. J. Briscoe *et al.*, *Nature* **398**, 622–627 (1999).
6. A. Pattyn, M. Hirsch, C. Goridis, J. F. Brunet, *Development* **127**, 1349–1358 (2000).
7. S. Guthrie, *Nat. Rev. Neurosci.* **8**, 859–871 (2007).
8. A. Prasad, M. Hollyday, *J. Comp. Neurol.* **307**, 237–258 (1991).
9. J. A. Markham, J. E. Vaughn, *J. Neurobiol.* **22**, 811–822 (1991).
10. W. A. Alaynick, T. M. Jessell, S. L. Pfaff, *Cell* **146**, 178–178.e1 (2011).
11. P. E. Phelps, R. P. Barber, J. E. Vaughn, *J. Comp. Neurol.* **330**, 1–14 (1993).
12. C. R. Anderson, *Neurosci. Lett.* **139**, 280–284 (1992).

13. J. S. Dasen, A. De Camilli, B. Wang, P. W. Tucker, T. M. Jessell, *Cell* **134**, 304–316 (2008).
14. J. R. Keast, *Int. Rev. Cytol.* **248**, 141–208 (2006).
15. J. R. Keast, *Neuroscience* **66**, 655–662 (1995).
16. A. Kuntz, R. L. Moseley, *J. Comp. Neurol.* **64**, 63–75 (1936).
17. W. C. De Groat, A. M. Booth, J. Krier, in *Integrative Functions of the Autonomic Nervous System*, C. M. Brooks, K. Koizumi, A. Sato, Eds. (University of Tokyo Press, Tokyo, 1979), pp. 234–245.
18. U. Ernsberger, H. Rohrer, *Cell Tissue Res.* **297**, 339–361 (1999).
19. K. Huber *et al.*, *Dev. Biol.* **380**, 286–298 (2013).
20. K. Tsarovina *et al.*, *Development* **131**, 4775–4786 (2004).
21. E. Doxakis, L. Howard, H. Rohrer, A. M. Davies, *EMBO Rep.* **9**, 1041–1047 (2008).
22. L. Huber, M. Ferdin, J. Holzmann, J. Stubbusch, H. Rohrer, *Dev. Biol.* **363**, 219–233 (2012).
23. C. L. Yntema, W. S. Hammond, *J. Exp. Zool.* **129**, 375–413 (1955).
24. V. Dyachuk *et al.*, *Science* **345**, 82–87 (2014).
25. I. Espinosa-Medina *et al.*, *Science* **345**, 87–90 (2014).
26. S. Nilsson, in *Autonomic Nerve Function in the Vertebrates*, *Zoophysiology*, vol. 13, D. S. Farner, Ed. (Springer-Verlag, New York, 1983), chap. 2.
27. C. Olsson *et al.*, *J. Comp. Neurol.* **496**, 787–801 (2006).
28. K. Fukai, H. Fukuda, *J. Physiol.* **362**, 69–78 (1985).
29. W. Jänig, *The Integrative Action of the Autonomic Nervous System: Neurobiology of Homeostatis* (Cambridge Univ. Press, Cambridge, UK, 2006).
30. W. C. de Groat, W. R. Saum, *J. Physiol.* **220**, 297–314 (1972).
31. A. Pattyn, X. Morin, H. Cremer, C. Goridis, J. F. Brunet, *Nature* **399**, 366–370 (1999).

PLANT SCIENCE

Phytochrome B integrates light and temperature signals in *Arabidopsis*

Martina Legris,[1] Cornelia Klose,[2]* E. Sethe Burgie,[3]* Cecilia Costigliolo Rojas,[1]* Maximiliano Neme,[1] Andreas Hiltbrunner,[2,4] Philip A. Wigge,[5] Eberhard Schäfer,[2,4]† Richard D. Vierstra,[3]† Jorge J. Casal[1,6]‡

Ambient temperature regulates many aspects of plant growth and development, but its sensors are unknown. Here, we demonstrate that the phytochrome B (phyB) photoreceptor participates in temperature perception through its temperature-dependent reversion from the active Pfr state to the inactive Pr state. Increased rates of thermal reversion upon exposing *Arabidopsis* seedlings to warm environments reduce both the abundance of the biologically active Pfr-Pfr dimer pool of phyB and the size of the associated nuclear bodies, even in daylight. Mathematical analysis of stem growth for seedlings expressing wild-type phyB or thermally stable variants under various combinations of light and temperature revealed that phyB is physiologically responsive to both signals. We therefore propose that in addition to its photoreceptor functions, phyB is a temperature sensor in plants.

Plants have the capacity to adjust their growth and development in response to light and temperature cues (*1*). Temperature-sensing helps plants determine when to germinate, adjust their body plan to protect themselves from adverse temperatures, and flower. Warm temperatures as well as reduced light resulting from vegetative shade promote stem growth, enabling seedlings to avoid heat stress and canopy shade from neighboring plants. Whereas light perception is driven by a collection of identified photoreceptors—including the red/far-red light–absorbing phytochromes; the blue/ultraviolet-A (UV-A) light–absorbing cryptochromes, phototropins, and members of the Zeitlupe family; and the UV-B–absorbing UVR8 (*2*)—temperature sensors remain to be established (*3*). Finding the identity (or identities) of temperature sensors would be of particular relevance in the context of climate change (*4*).

Phytochrome B (phyB) is the main photoreceptor controlling growth in *Arabidopsis* seedlings exposed to different shade conditions (*5*). Like others in the phytochrome family, phyB is a homodimeric chromoprotein, with each subunit harboring a covalently bound phytochromobilin chromophore. phyB exists in two photo-interconvertible forms: a red light–absorbing Pr state that is biologically inactive and a far-red light–absorbing Pfr state that is biologically active (*6*, *7*). Whereas Pr arises upon assembly with the bilin, formation of Pfr requires light, and its levels are strongly influenced by the red/far-red light ratio. Consequently, because red light is absorbed by photosynthetic pigments, shade light from neighboring vegetation has a strong impact on Pfr levels by reducing this ratio (*8*). phyB Pfr also spontaneously reverts back to Pr in a light-independent reaction called thermal reversion (*9–11*). Traditionally, thermal reversion was assumed to be too slow relative to the light reactions to affect the Pfr status of phyB, even under moderate irradiances found in natural environments, but two observations contradict this view. First, the formation of phyB nuclear bodies, which reflects the status of Pfr, is affected by light up to irradiances much higher than expected if thermal reversion were slow (*12*). Second, it is now clear that thermal reversion occurs in two steps. Although the first step, from the Pfr:Pfr homodimer (D2) to the Pfr:Pr heterodimer (D1), is slow (k_{r2}), the second step, from the Pfr:Pr heterodimer to the Pr:Pr homodimer (D0), is almost two orders of magnitude faster (k_{r1}) (Fig. 1A) (*11*).

Physiologically relevant temperatures could change the magnitude of k_{r1} and consequently affect Pfr and D2 levels, even under illumination (Fig. 1A). To test this hypothesis, we used in vitro and in vivo spectroscopy and analysis of phyB nuclear bodies by means of confocal microscopy. For the first of these approaches, we produced recombinant full-length phyB bearing its phytochromobilin chromophore. When irradiated under continuous red light, the in vitro absorbance at 725 nm reached lower values at higher temperatures, which is indicative of reduced steady-state levels of Pfr (Fig. 1, B and C). We calculated the differences between the steady-state absorbance spectra in darkness and continuous red light (Δ absorbance). The amplitude between the maximum and minimum peaks of Δ absorbance, which represents the amount of Pfr, strongly decreased between 10 and 30°C (Fig. 1, D and E). This characteristic of phyB differs from the typical behavior

[1]Fundación Instituto Leloir, Instituto de Investigaciones Bioquímicas de Buenos Aires–Consejo Nacional de Investigaciones Científicas y Técnicas (CONICET), 1405 Buenos Aires, Argentina. [2]Institut für Biologie II, University of Freiburg, Schaenzlestrasse 1, D-79104 Freiburg. [3]Department of Biology, Washington University in St. Louis, Campus Box 1137, One Brookings Drive, St. Louis, MO 63130, USA. [4]BIOSS Centre for Biological Signaling Studies, University of Freiburg, Schaenzlestrasse 18, 79104 Freiburg, Germany. [5]Sainsbury Laboratory, Cambridge University, 47 Bateman Street, Cambridge CB2 1LR, UK. [6]Instituto de Investigaciones Fisiológicas y Ecológicas Vinculadas a la Agricultura (IFEVA), Facultad de Agronomía, Universidad de Buenos Aires and CONICET, Avenida San Martín 4453, 1417 Buenos Aires, Argentina.
*These authors contributed equally to this work. †These authors contributed equally to this work. ‡Corresponding author. Email: casal@ifeva.edu.ar

Editor's Summary

Sacral neurons reassigned

The autonomic nervous system regulates the function of internal organs such as the gut. The parasympathetic and sympathetic arms of this system tend to operate antagonistically. Espinosa-Medina *et al.* used anatomical and molecular analyses to reevaluate the assignment of neurons in the sacral autonomic nervous system (see the Perspective by Adameyko). Previously categorized as parasympathetic, these neurons are now identified as sympathetic. The results resolve a persistent confusion about how the two systems developed and open the avenue to more predictable outcomes in developing treatments targeted to the pelvic autonomic nervous system.

Science, this issue p. 893; see also p. 833

Article Tools	Visit the online version of this article to access the personalization and article tools: http://science.sciencemag.org/content/354/6314/893
Permissions	Obtain information about reproducing this article: http://www.sciencemag.org/about/permissions.dtl